ACTA ET COMMENTATIONES UNIVERSITATIS TARTUENSIS DE MATHEMATICA
Volume 22, Number 1, June 2018
Available online at http://acutm.math.ut.ee

Biot number effect on MHD flow and heat transfer of nanofluid with suspended dust particles in the presence of nonlinear thermal radiation and non-uniform heat source/sink

B. J. Gireesha, R. S. R. Gorla, M. R. Krishnamurthy, and B. C. Prasannakumara

Abstract. This paper considers the problem of steady, boundary layer flow and heat transfer of dusty nanofluid over a stretching surface in the presence of non-uniform heat source/sink and nonlinear thermal radiation with Biot number effect. The base fluid (water) is considered with silver (Ag) nanoparticles along with suspended dust particles. The governing equations in partial form are reduced to a system of non-linear ordinary differential equations using suitable similarity transformations. An effective Runge–Kutta–Fehlberg fourth-fifth order method along with shooting technique is used for the solution. The effects of flow parameters such as nanofluid interaction parameter, magnetic parameter, solid volume fraction parameter, Prandtl number, heat source/sink parameters, radiation parameter, temperature ratio parameter and Biot number on the flow field and heat-transfer characteristics were obtained and are tabulated. Useful discussions were carried out with the help of plotted graphs and tables. Under the limiting cases, comparison with the existing results was made and found to be in good agreement.

1. Introduction

The problems of boundary layer flow and heat transfer over a stretching surface have many applications in polymer industry, fibre industry, chemical drying, paper production, glass blowing, etc. In all these cases, the quality of the final product depends on the rate of heat transfer at the stretching surface. The heat-transfer analysis of boundary-layer flow with radiation

Received February 17, 2017.
2010 *Mathematics Subject Classification.* 76T15; 80A20; 76D05.
Key words and phrases. Nanoparticle; dusty fluid; nonlinear thermal radiation; nonuniform heat source/sink; convective boundary condition; numerical solution.
http://dx.doi.org/10.12697/ACUTM.2018.22.09
Corresponding author: B. C. Prasannakumara

is also important in electrical power generation, astrophysical flows, solar power technology, space vehicle re-entry and other industrial applications. Sakiadis [33] was the first person to present boundary layer flow over a continuous solid surface moving with constant speed. The flow of an incompressible viscous fluid over a linearly stretching sheet has been studied by Crane [5], who obtained an exact solution for the flow field. Cortell [3] studied the flow of an electrically conducting power-law fluid in the presence of a uniform transverse magnetic field over a stretching sheet. Shehzad et al. [36] have studied heat and mass transfer analysis combined with Soret and Dufour effects in boundary layer flow of Jeffrey fluid with convective thermal condition. Mabood et al. [17] reported on steady two-dimensional hydromagnetic mixed convective heat and mass transfer flow of a micropolar fluid over a stretching sheet embedded in a non-Darcian porous medium with thermal radiation and non-uniform heat source/sink.

Nanofluids are innovative coolants with more effective cooling properties compared to the conventional fluids such as water and oil. Unfortunately the viscosity of the nanofluid is higher than the base fluid. Thus viscosity affects directly the pressure drop and pumping consumption of the system. Greater thermal conductivity, excellent stability and negligible increasing pressure loss are some important characteristics of nanofluids that are mentioned in the literature. One can find a large number of works on different aspects of the nanofluids such as their thermal conductivity ([22], [9]), dynamic viscosity ([25], [8]), and thermal expansion [24]. An exponential increase in the number of experimental works on applications of nanofluids in forced convection regimes is observed in the recent years. Wen and Ding [38] conducted an experiment on convective heat transfer of alumina-water nanofluids through a copper tube in laminar flow regime. Pak and Cho [26] experimentally investigated the flow behavior and convective heat transfer of TiO_2 and Al_2O_3 water based nanofluids through a horizontal tube. They have presented the first regression correlation to predict nanofluid Nusselt number which is independent of nanoparticles solid volume fraction. An experimental study of Copper-water nanofluids in a straight tube with constant heat flux wall and convective heat transfer has been reported by Xuan and Li [39]. Their funding showed that the heat transfer rate of nanofluid is greater than pure water.

In the support of experimental work, Sheikholeslami and Ganji [37] theoretically investigated the heat transfer of Cu-water nanofluid flow which is squeezed between parallel plates. Elazem et al. [7] have numerically investigated the effect of radiation on the steady MHD flow and heat transfer of Cu-water and Ag-water nanofluids over a stretching sheet. Khare [16] reported the partial slip effect on MHD flow and heat transfer of Ag-water nanofluid over a stretching sheet. Recently, Hedayati et al. [14] show the

effects of nanoparticle migration and asymmetric heating on the forced convective heat transfer of Al_2O_3-water nanofluid in microchannels. The natural convection in an open cavity with non uniform thermal boundary condition and the cavity is filled with Al_2O_3-water nanofluid in the presence of magnetic field and heat generation or absorption was investigated by Mahmoud [18].

The study of the flow of dusty fluid has important applications in the fields of fluidization, combustion, in cooling systems, centrifugal separation of matter from fluid, petroleum industry, and purification of crude oil, electrostatic precipitation, polymer technology and fluid droplets sprays. Initially, Saffman [32] described the fluid-particle system and obtained the equation of motion for fluid carrying the dust particles. The heat transfer effects on dusty gas flow past a semiinfinite isothermal inclined plate was analyzed by Palani and Ganesan [27]. Nandkeolyar et al. [23] considered the natural convection boundary layer flow of a viscous, incompressible, and electrically conducting dusty fluid past an impulsively moving vertical plate with ramped temperature in the presence of thermal radiation and transverse magnetic field. The problem of two-dimensional mixed convective flow a dusty fluid over a stretching sheet in the presence of thermal radiation and space dependent heat source/sink was investigated by Gireesha et al. [10]. Recenty, Gorla et al. [11] studied the effect of non-uniform heat source/sink and viscous dissipation on hydromagnetic fluid flow and heat transfer of nanofluid with fluid particle suspension over an exponential stretching sheet.

Convective heat transfer mobilized substantial interest owing to its importance in industrial and environmental technologies including energy storage, gas turbines, nuclear plants, rocket propulsion, geothermal reservoirs, and photovoltaic panels etc. Recently, Ishak [15] reported the steady laminar boundary layer flow over a permeable flat plate with convective boundary conditions. The effect of thermal buoyancy along a stationary vertical plate with a uniform free stream flow were studied by Makinde and Olanrewaju [19]. Bég et al. [1] studied the mixed magneto-convective flow of an electrically conducting flow along a moving radiating vertical flat plate with hydrodynamic slip and thermal convective boundary conditions. Ramesha and Gireesha [30] examined the heat source/sink effects on the steady boundary layer flow of a Maxwell fluid over a stretching sheet with convective boundary condition in the presence of nanoparticles. The effects of slip and convective heat boundary conditions on steady two dimensional boundary layer flow of a nanofluid over a stretching sheet in the presence of blowing/suction was reported by Malvandi et al. [20].

In the above mentioned studies, some of (see [7], [23] and [10]) were confined to the linear approximation for the radiative heat transfer effects

which are valid for small temperature differences. It is difficult to construct a system in scientific and engineering applications in which the working fluids will have a small temperature differences. Therefore, the heat transfer with nonlinear radiation has been recently presented by some researchers. The Sakiadis flow with nonlinear Rosseland thermal radiation was considerd by Pantokratoras and Fang [28]. Unlike, small temperature difference within the fluid, they have assumed large temperature differences. Cortell [4] numerically explored the radiation effect on fluid flow and heat transfer over a stretching sheet using nonlinear Rosseland approximation. Hayat et al. [13] analyzed the nonlinear thermal radiation effect on magnetohydrodynamic three-dimensional flow of couple stress nanofluid in the presence of thermophoresis and Brownian motion. Recently, Prasannakumara et al. [29] investigated the effects of chemical reaction and thermal radiation on Williamson nanofluid slip flow over a stretching sheet using nonlinear Rosseland approximation.

The present study aims to investigate the effects of nonuniform heat source/sink, nonlinear thermal radiation and Biot number on dusty fluid containing Ag-water nanoparticles over a stretching sheet. The governing equations of the flow are solved numerically using the Runge–Kutta–Fehlberg fourth-fifth order method along with the shooting technique. Effect of governing parameters on velocity, temperature, friction factor and Nusselt number is discussed with the aid of presented graphs. Comparison of the obtained results are made with the existing results.

2. Mathematical formulation

Consider a steady, laminar, two-dimensional boundary layer flow and heat transfer of an incompressible dusty fluid combined with Ag nanoparticles past a stretching sheet. The sheet coincides with the plane $y = 0$ and the flow is confined to $y > 0$. The flow is generated due to linear stretching of the sheet caused by the simultaneous applications of two equal and opposite forces along the x-axis as shown in the Figure 1 (see Appendix 2). A uniform magnetic field B_0 is assumed to be applied in the y-direction. Keeping the origin fixed, the sheet is then stretched with a velocity $U_w(x) = bx$ where $b > 0$ is the stretching rate and x is the coordinate measured along the stretching surface, varying linearly with a distance from the slit. The ambient fluid temperature is a constant T_∞. The sheet surface temperature is maintained by convective heat transfer at a certain value T_f, which is to be determined later. The fluid is a water based dusty fluid containing Ag nanoparticles. The nanoparticles are assumed to have a uniform shape and size. Moreover, it is assumed that both the fluid phase and nanoparticles are in thermal equilibrium state.

Under usual boundary layer approximations, the flow governing equations of nanofluid phase and dust phase are given by

$$\frac{\partial u}{\partial x}+\frac{\partial v}{\partial y}=0, \tag{2.1}$$

$$u\frac{\partial u}{\partial x}+v\frac{\partial u}{\partial y}=\frac{\mu_{nf}}{\rho_{nf}}\frac{\partial^2 u}{\partial y^2}+\frac{KN}{\rho_{nf}}(u_p-u)-\frac{\sigma B_0^2}{\rho_{nf}}u, \tag{2.2}$$

$$\frac{\partial u_p}{\partial x}+\frac{\partial v_p}{\partial y}=0, \tag{2.3}$$

$$u_p\frac{\partial u_p}{\partial x}+v_p\frac{\partial u_p}{\partial y}=\frac{K}{m}(u-u_p), \tag{2.4}$$

$$(\rho c_p)_{nf}\left[u\frac{\partial T}{\partial x}+v\frac{\partial T}{\partial y}\right]=k_{nf}\frac{\partial^2 T}{\partial y^2}+\frac{Nc_{pf}}{\tau_T}(T_p-T) + \frac{N}{\tau_v}(u_p-u)^2-\frac{\partial q_r}{\partial y}+q''', \tag{2.5}$$

$$u_p\frac{\partial T_p}{\partial x}+v_p\frac{\partial T_p}{\partial y}=\frac{c_{pf}}{c_{mf}\tau_T}(T-T_p), \tag{2.6}$$

where x and y respectively represent coordinate axes along the continuous surface in the direction of motion and perpendicular to it. Here (u, v) and (u_p, v_p) denote the velocity components of the nanofluid and dust phases along the x and y directions, respectively, N is the number density of dust particle, $K = 6\pi\mu_{nf}r$ is the Stokes drag constant, r is the radius of dust particle, σ is the electrical conductivity, m is the mass concentration of dust particles, ρ_{nf} is the effective density of nanofluid, μ_{nf} is the effective dynamic viscosity of nanofluid which are given by (see [34])

$$\rho_{nf}=(1-\phi)\rho_f+\phi\rho_s,\quad \mu_{nf}=\frac{\mu_f}{(1-\phi)^{2.5}}, \tag{2.7}$$

where ϕ is the solid volume fraction of nanofluid, ρ_f is the density of base fluid, ρ_s is the density of the nanoparticle, and μ_f is the dynamic viscosity of the base fluid.

In equations (2.5) and (2.6), T and T_p represent the temperatures of the fluid and dust particle inside the boundary layer, c_{pf} and c_{mf} are the specific heat of the fluid and dust particles, τ_T is the thermal equilibrium time, i.e., the time required by a dust cloud to adjust its temperature to that of the fluid, τ_v is the relaxation time of the dust particle, that is, the time required by a dust particle to adjust its velocity relative to the fluid, k_{nf} is the thermal conductivity, and $(\rho c_p)_{nf}$ is heat capacity of the nanofluid, which are given by (see [34])

$$\frac{k_{nf}}{k_f}=\frac{k_s+2k_f-2\phi(k_f-k_s)}{k_s+2k_f+2\phi(k_f-k_s)},\quad (\rho c_p)_{nf}=(1-\phi)(\rho c_p)_f+\phi(\rho c_p)_s, \tag{2.8}$$

where $(\rho c_p)_f$ is the heat capacity of the base fluid, $(\rho c_p)_s$ is the heat capacity of the nanoparticle, k_f is the thermal conductivity of the base fluid, and k_s is the thermal conductivity of nanoparticle. The corresponding boundary

conditions are given by

$$u = U_w, \quad v = 0, \quad k_{nf}\frac{\partial T}{\partial y} = h_f(T_f - T) \ \text{ at } \ y = 0,$$
$$u \to 0, \quad u_p \to 0, \quad v_p \to v, \quad T \to T_\infty, \quad T_p \to T_\infty \ \text{ as } \ y \to \infty. \tag{2.9}$$

Here q''' is the space and temperature dependent internal heat generation/absorption (non uniform heat source/sink) which can be expressed as

$$q''' = \frac{k_{nf}U_w(x)}{x\nu_f}[A_1(T_f - T_\infty)f'(\eta) + B_1(T - T_\infty)], \tag{2.10}$$

where T_f and T_∞ denote the temperature at the wall and at large distance from the wall, respectively, A_1 and B_1 are the parameters of the space and temperature dependent internal heat generation/absorption. It is to be noted that A_1 and B_1 are positive to internal heat source and negative to internal heat sink.

Unlike the linearized Rosseland approximation, we use nonlinear Rosseland diffusion approximation from which one can obtain results for both small and large differences between T_f and T_∞.

Using Rosseland (see [31], [35]) approximation for radiation, the radiative heat flux q_r is simplified as

$$q_r = -\frac{4\sigma^*}{3k^*}\frac{\partial T^4}{\partial y} = -\frac{16\sigma^*}{3k^*}T_\infty 3\frac{\partial T}{\partial y}, \tag{2.11}$$

where σ^* is the Stefan–Boltzmann constant and k^* is the mean absorption coefficient. Now after simplification, equation (2.5) takes the form

$$(\rho c_p)_{nf}\left[u\frac{\partial T}{\partial x} + v\frac{\partial T}{\partial y}\right] = \frac{\partial}{\partial y}\left[\left(k_{nf} + \frac{16\sigma^* T_\infty^3}{3k^*}\right)\frac{\partial T}{\partial y}\right] + \frac{Nc_{pf}}{\tau_T}(T_p - T) + \frac{N}{\tau_v}(u_p - u)^2 + q'''. \tag{2.12}$$

To convert the governing equations into a set of similarity equations, introduce the following similarity transformation:

$$u = bxf'(\eta), \quad v = \sqrt{-b\nu_f}f(\eta), \quad \eta = \sqrt{\frac{b}{\nu_f}}y, \quad u_p = bxF'(\eta),$$
$$v_p = \sqrt{-b\nu_f}F(\eta), \quad \theta(\eta) = \frac{T - T_\infty}{T_f - T_\infty}, \quad \text{and} \quad \theta_p(\eta) = \frac{T_p - T_\infty}{T_f - T_\infty}. \tag{2.13}$$

with $T = T_f(1 + (\theta_w - 1)\theta)$ and $\theta_w = \frac{T_f}{T_\infty}$, $\theta_w > 1$, the temperature ratio parameter. Making use of the transformations (2.14), equations (2.1) and (2.3) are identically satisfied and equations (2.2), (2.4), (2.6), and (2.13) take the form

$$f''' + (1-\phi)^{2.5}\left[(1-\phi) + \phi\frac{\rho_s}{\rho_f}\right](ff'' - f'^2) + (1-\phi)^{2.5} \times \left[l\beta_v(F' - f') - Mf'\right] = 0, \tag{2.14}$$

$$FF'' - [F']^2 + \beta_v[f' - F'] = 0, \tag{2.15}$$

$$\frac{k_{nf}}{k_f}\left[1 + Nr(1 + (\theta_w - 1)\theta)^3\theta'\right]' + Pr\left[(1-\phi) + \phi\frac{(\rho c_p)_s}{(\rho c_p)_f}\right] f\theta' + \frac{lPr\beta_T}{m}[\theta_p - \theta] + \frac{lPrEc\beta_v}{m}\left[F' - f'\right]^2 + \frac{k_{nf}}{k_f}[A_1 f' + B_1\theta] = 0, \tag{2.16}$$

$$F\theta_p' + \gamma\beta_T[\theta - \theta_p] = 0. \tag{2.17}$$

The corresponding boundary conditions will take the following form:

$$f(0) = 0, \quad f'(0) = 1, \quad \theta'(0) = -B_i(1 - \theta(0)),$$
$$f'(\infty) = 0, \quad F'(\infty) = 0, \quad F(\infty) = f(\infty), \quad \theta(\infty) = 0, \quad \theta_p(\infty) = 0. \tag{2.18}$$

Here a prime denotes differentiation with respect to η, the number $l = mN/\rho_f$ is the mass concentration of particles, $\tau_v = m/K$ is the relaxation time of the dust particle, $\beta_v = 1/\tau_v b$ is the fluid-particle interaction parameter for velocity, $M = \frac{\sigma B_0^2}{\rho_f b}$ is the magnetic parameter, $\beta_T = \frac{1}{b\tau_T}$ is the fluid-particle interaction parameter for temperature, $Pr = \frac{(\mu c_p)_f}{k_f}$ is the Prandtl number, $Ec = \frac{{U_w}^2}{(T_f - T_\infty)c_{pf}}$ is the Eckert number, $Nr = \frac{16\sigma^* T_\infty^3}{3k_{nf}k^*}$ is the radiation parameter, $\gamma = \frac{c_{pf}}{c_{mf}}$ is the ratio of specific heat, and $B_i = \sqrt{\frac{\nu_f}{b}}\frac{h_f}{k_{nf}}$ is the Biot number.

The physical quantities of interest are the skin friction coefficient (C_{fx}) and the local Nusselt number (Nu_x), which are defined as

$$C_{fx} = \frac{\tau_w}{\rho_f U_w^2}, \quad Nu_x = \frac{xq_w}{k_{nf}(T_f - T_\infty)}\frac{\partial T}{\partial y} \quad \text{at} \quad y = 0, \tag{2.19}$$

where the surface shear stress τ_w and the surface heat flux q_w are given by

$$\tau_w = \mu_f\left(\frac{\partial u}{\partial y}\right) \quad \text{and} \quad q_w = -k_{nf}\left(\frac{\partial T}{\partial y}\right) + (q_r)w \quad \text{at} \quad y = 0, \tag{2.20}$$

with μ_{nf} and k_{nf} being the dynamic viscosity and thermal conductivity of the nanofluids, respectively. Using the similarity transformations from (2.13), we obtain

$$\sqrt{Re_x}C_{fx} = \frac{1}{(1-\phi)^{2.5}}f''(0), \qquad \frac{Nu_x}{\sqrt{Re_x}} = -\frac{k_{nf}}{k_f}(1 + Nr\theta_w^3)\theta'(0), \tag{2.21}$$

where $Re = \frac{bx^2}{\nu_f}$ is the Reynolds number.

3. Numerical procedure

The resultant ordinary differential equations are coupled and nonlinear in nature, therefore, a closed-form solution may not be possible. Thus, the RKF-45 method with the shooting technique is used in the present study

to solve the boundary-layer equations (2.14)–(2.17) when subjected to the boundary conditions equation (2.18). The shooting technique is an iterative algorithm that attempts to identify appropriate initial conditions for a relevant initial value problem that provides the solution to the original boundary value problem. The shooting method is based on Maple implementation "shoot" and its detailed procedure can be found in Meade et al. [21]. This algorithm is proven to be precise and accurate, and it has been successfully used to solve a wide range of nonlinear problems in transport phenomena, especially flow and heat transfer problems. In this study, the relative error tolerance to 10^{-6} is considered. The asymptotic boundary conditions at η_∞ are replaced by η_6, in accordance with $f'\eta_{max} = f''\eta_{max} = \theta\eta_{max} = 0$, where η_{max} is a sufficiently large value of η at which the boundary conditions (2.18) are asymptotically satisfied. The thermo physical properties of water and Ag nanoparticle are shown in Table I (see Appendix 1).

The accuracy of the aforementioned numerical method was validated by direct comparisons with the numerical results corresponding to the values of skin friction coefficient $[-f''(0)]$ with those reported by Das [6] for different values of volume fraction of nanoparticles (ϕ) by keeping $l = 0$ and $M = 0$. Further, we have made a comparison of values of heat transfer coefficient $[-\theta'(0)]$ reported earlier by Grubka and Bobba [12] and Chen [2] for various values of Prandtl number in the absence of the nanoparticle volume fraction and mass concentration of particles parameter $\phi = l = 0$, and they are presented in Tables II and III, respectively. It can be seen from these tables that an excellent agreement between the results exists. This favorable comparison lends confidence in the numerical results to be reported in the next section.

4. Results and discussion

MHD flow and heat transfer of dusty fluid with Ag-water nanoparticles in the presence of nonlinear thermal radiation and nonuniform heat source/sink over a stretching surface with convective boundary condition have been studied. The purpose of this section is to analyze the effects of various physical parameters such as magnetic parameter (M), fluid particle interaction parameter for velocity (β_v), solid volume fraction parameter (ϕ), mass concentration particle parameter (l), radiation parameter (Nr), temperature ratio parameter (θ_w), Biot number (B_i), Eckert number (Ec), Prandtl number (Pr), and heat source/sink parameters (A_1 and B_1) on the velocities and temperature fields as well as skin friction coefficient and local Nusselt number profiles. Therefore, for such objective, Figures 2–18 have been plotted. In numerical computations throughout, we employed $M = 0.3$, $\beta_v = 0.5$, $\phi = 0.2$, $A_1 = B_1 = 0.5$, $\theta_w = 1.2$, $Nr = 1.5$, $B_i = 0.2$, $l = 0.2$, and $Pr = 6.2$. The numerical result of skin friction co-efficient and rate of

heat transfer are examined for different values physical parameters, which are tabulated in Tables IV and V.

Figures 2 and 3 illustrate the influence of the magnetic parameter (M) on the velocity and temperature profiles in the boundary layer, respectively. An application of a transverse magnetic field to an electrically conducting fluid gives rise to a resistive-type force called the Lorentz force. This force has the tendency to slow down the motion of the fluid in the boundary layer and to increase its temperature. Also, the effects on the flow and thermal fields become more so as the strength of the magnetic field increases.

The variation of velocity and temperature profiles with η for different values of the nanofluid interaction parameter for velocity (β_v) for both nanofluid and dust phases are illustrated in Figures 4 and 5, respectively. It is noticed from these figures that the velocity profiles decrease with increasing values of β_v for nanofluid phase and increase for dust phase in the boundary layer. The increasing values of β_v reduce the velocity $f'(\eta)$ and thereby increase the boundary layer thickness. For increasing values of β_v the temperature profile increases for both the phases and also one can observed that nanofluid phase temperature is higher than that of dust phase, which is shown in Figure 5.

The effect of mass concentration of particle parameter (l) for both nanofluid and dust phase of velocity and temperature profile are depicted in Figures 6 and 7. From these plots, we observed that, an increase in mass concentration of particles, the velocity profile increases and temperature profile decreases for both of the phases. Moreover, it is interesting to note that the value $l = 0$ corresponds to the ordinary viscous nanofluid.

The effect of nanoparticle volume fraction parameter (ϕ) on velocity and temperature profiles for both nano fluid and dust phases are, respectively, illustrated graphically through Figures 8 and 9. From these figures, it is observed that as the volume fraction of nanoparticles increases from 0 to 0.2, velocity profile for both nanofluid and dust phase decreases inside the boundary layer and temperature profile increases for both of the phases.

Figures 10 and 11 show the temperature profiles $\theta(\eta)$ and $\theta_p(\eta)$ versus η for different values of A_1 and B_1. From these plots it is evident that increase in A_1 [$A_1 > 0$ (heat source)] results in the enhancement of both fluid and dust phase temperature, whereas $A_1 < 0$ (heat sink) leads to decrease in the thermal boundary layer. It is due to the fact that for $A_1 > 0$, the thermal boundary layer generates the energy and obviously energy is absorbed for decreasing values of A_1 resulting in temperature dropping significantly near the boundary layer. The similar effect is observed from the Figure 11 for the effect of temperature-dependent heat source/sink parameter B_1.

Figure 12 represents the effect of radiation parameter (Nr) on temperature profiles for both nanofluid and dust phases. Numerically increasing the radiation parameter enhances the heat transfer, physically increasing the radiation parameter produces a significant increase in the thickness of

thermal boundary layer. In fact, the radiation parameter decreases the fluid temperature. This is because as the radiation parameter increases, the mean Rosseland absorption co-efficient k^* decreases (for some thermal conductivity k_{nf}). Hence the thermal radiation factor is better suitable for cooling process.

Figure 13 illustrates the effect of temperature ratio parameter (θ_w) on temperature profile for both nanofluid and dust phases. We noticed that the increase in temperature ratio parameter increases the thermal state of the fluid, resulting in increase temperature profiles. Physically, the fluid temperature is much higher than the ambient temperature for increasing values of (θ_w), which increases the thermal state of the fluid.

In Figure 14, the variation of temperature $\theta(\eta)$ and $\theta_p(\eta)$ with η for various values of the Biot number (B_i) is presented. It is observed that temperature fields $\theta(\eta)$ and $\theta_p(\eta)$ increase rapidly near the boundary by increasing Biot number. This is because of convective heat exchange at the plate surface leading to an increase in thermal boundary layer thickness.

Figure 15 is plotted for the temperature distribution for different values of Eckert number (Ec). Here the temperature of both nanofluid and dust phase increases with the increase in the value of Ec. It is because the heat energy is stored in the liquid due to frictional heating and this is true in the both cases.

The temperature profile for various values of Prandtl number (Pr) is plotted for both nanofluid and dust phases in Figure 16. From this figure it reveals that the temperature decreases with the increase in the value of Pr. Physically an enhancement in the Prandtl number corresponds to weaker thermal diffusivity. It is a well-known fact that the fluids with weaker thermal diffusivity have lower temperature. Such weaker thermal diffusivity shows a reduction in the temperature and thermal boundary layer thickness. Hence Prandtl number can be used to increase the rate of cooling.

Figure 17 depicts the Nusselt number effect on various values of solid volume fraction parameter (ϕ) versus magnetic parameter (M). From this plot we observed that the temperature gradient increases for increasing values of (ϕ). Similarly, the different values of radiation parameter (Nr) versus Biot number (B_i) of Nusselt number for linear and nonlinear Rosseland approximation are illustrated in Figure 18. Here, the Nusselt number increases for increasing values of Nr.

5. Conclusions

A mathematical analysis has been carried out to study the effects of nonlinear radiation, nonuniform heat source/sink and Biot number on hydromagnetic flow and heat transfer of dusty fluid over a stretching sheet combined with Ag-water nanoparticle. Some of the important observations of our analysis obtained by the graphical representation are reported as follows.

- The effect of magnetic parameter is to increase the temperature distribution in the flow region for both nanofluid and dust particle phases.
- The velocity of nanofluid and dust phases decreases while the temperature of nanofluid and dust phases increases as ϕ increases.
- The mass concentration particle parameter increases the velocity and decreases the temperature profiles in the flow region for both nanofluid and dust phases.
- The temperature of nanofluid and dust phases increases with increasing values of Nr, θ_w, Ec, and B_i.
- Temperature of nanofluid and dust phase decreases with increasing values of Pr.
- For silver (Ag) nanoparticles, the thermal conductivity is higher than other particles.
- The nanofluid phase temperature is higher than that of the dust phase.
- It is found that the dusty fluids with Ag nanoparticles have the appreciable cooling performance.

Appendix 1. Tables

Table I. Thermo physical properties of water and nanoparticles.

	$\rho(kg/m^3)$	$C_p(j/kgk)$	$k(W/mk)$
pure water (H_2O)	997.1	4179	0.613
Silver (Ag)	10500	235	429

Table II. Comparison results for skin friction co-efficient $(-f''(0))$ in the case of $\beta_v = M = 0$ and $l = 0$.

	$-f''(0)$	
ϕ	Das et al [6]	Present result
0.0	1.0014	1.00142
0.1	1.1752	1.17531
0.2	1.2183	1.21842

Table III. Values of $\theta'(0)$ for several values of Prandtl number and magnetic parameter in the absence of β, β_T, Ec, and ϕ.

Pr	Grubka et al [12]	Chen [2]	Present study
0.72	1.0885	1.0885	1.0884
2 1.0	1.3333	1.3333	1.3333
1.0	2.5097	2.5097	2.5096
10.0	4.7969	4.7968	4.7968

Table IV. Values of skin friction coefficient and Nusselt number for various values of the parameters when $Nr = 1.5,\ A_1 = B_1 = 0.5,\ B_i = 0.2,\ Pr = 6.2$, and $Ec = 0.5$.

						Nonlinear thermal radiation	Linear thermal radiation
β_v	β_T	l	M	ϕ	$\sqrt{Re_x}C_{fx}$	$Nu_x/\sqrt{Re_x}$	$Nu_x/\sqrt{Re_x}$
0					2.7106	1.3110	0.3676
0.3					2.7062	1.2545	0.3514
0.6					2.6961	1.2357	0.3459
	0.2				2.6999	0.9808	0.2744
	0.4				2.6999	1.1559	0.3238
	0.6				2.6999	1.2398	0.3471
		0.3			2.6945	1.2904	0.3607
		0.6			2.6782	1.3508	0.3768
		0.9			2.6619	1.3731	0.3827
			0		2.6010	1.2369	0.3463
			0.3		2.6999	1.2398	0.3471
			0.6		2.7952	1.2425	0.3479
				0	1.5055	0.5836	0.1633
				0.1	2.0469	0.8458	0.2367
				0.2	2.6999	1.2398	0.3471

Table V. Values of Nusselt number for different values of the parameters when $\beta_v = 0.5,\ \phi = 0.2$, and $M = 0.3$.

						Nonlinear thermal radiation	Linear thermal radiation
A_1	B_1	Nr	Pr	B_i	Ec	$Nu_x/\sqrt{Re_x}$	$Nu_x/\sqrt{Re_x}$
-0.5						1.4405	0.4033
0						1.3389	0.3752
0.5						1.2398	0.3471
	-0.5					1.2977	0.3631
	0					1.2718	0.3559
	0.5					1.2398	0.3471
		1				0.9507	0.3500
		1.5				1.2398	0.3471
		2				1.5230	0.3442
			3.2			1.0661	0.2999
			4.2			1.1501	0.3228
			5.2			1.2030	0.3471
				2		4.7458	1.4815
				5		5.7032	1.8942
				10		6.0936	2.0880
					0.5	4.7458	0.3471
					1	4.4975	0.3270
					2	4.0102	0.2867

Appendix 2: Figures

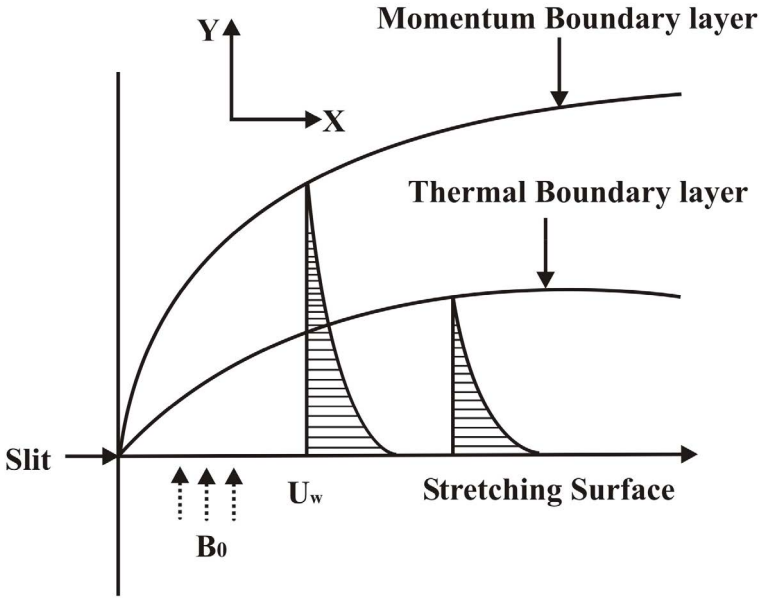

Figure 1. Schematic representation of the flow diagram.

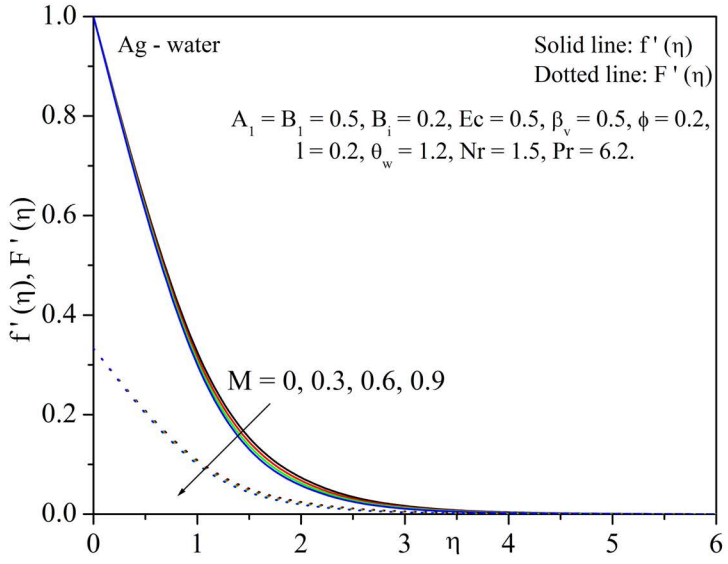

Figure 2. Velocity profile for various values of magnetic parameter (M).

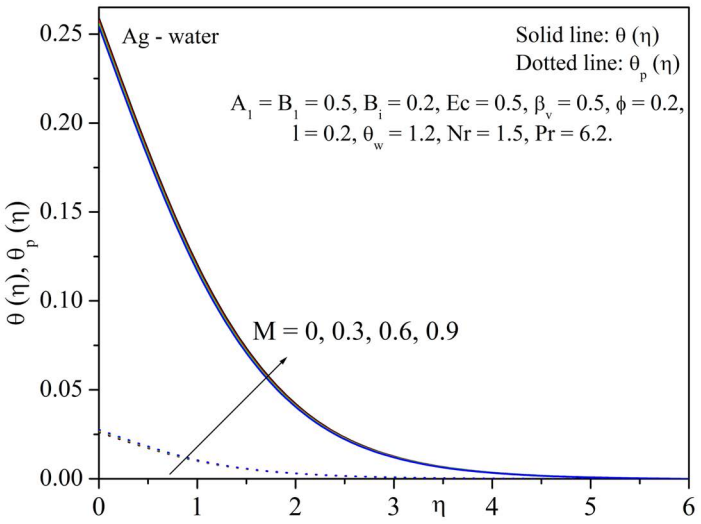

Figure 3. Temperature profile for various values of magnetic parameter (M).

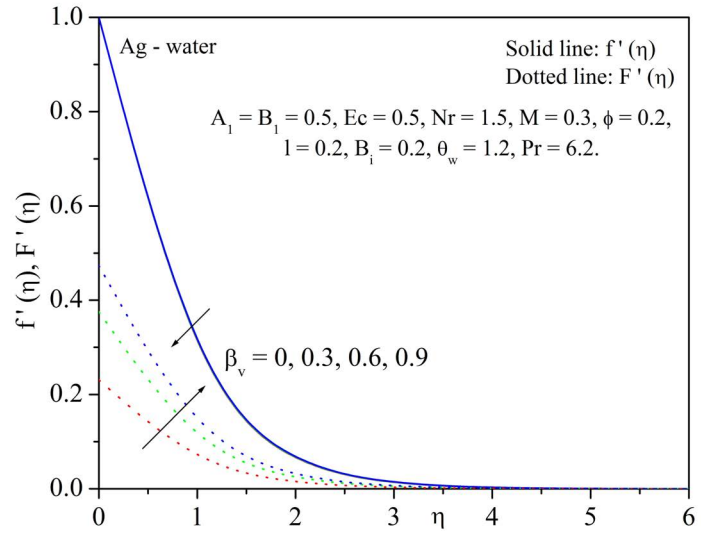

Figure 4. Velocity profile for various values of velocity fluid particle interaction parameter (β_v).

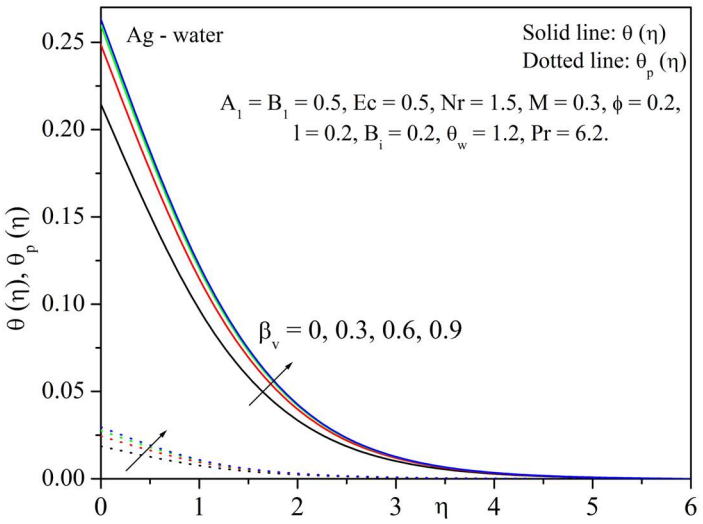

Figure 5. Temperature profile for various values of velocity fluid particle interaction parameter (β_v).

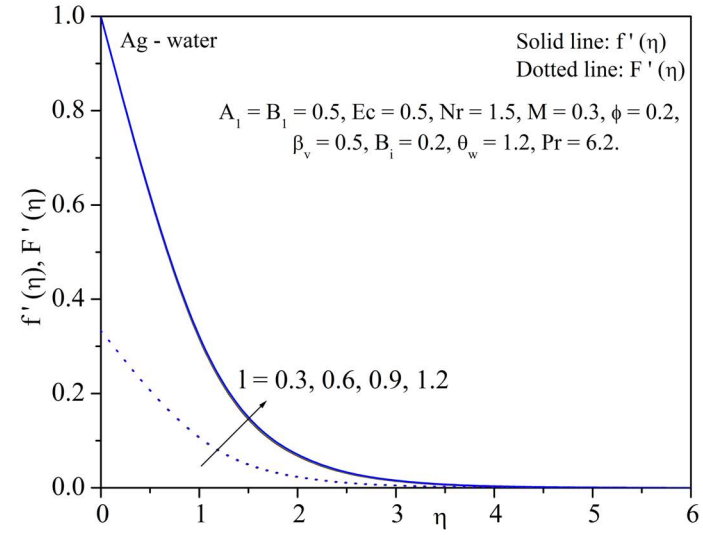

Figure 6. Velocity profile for various values of mass concentration particle parameter (l).

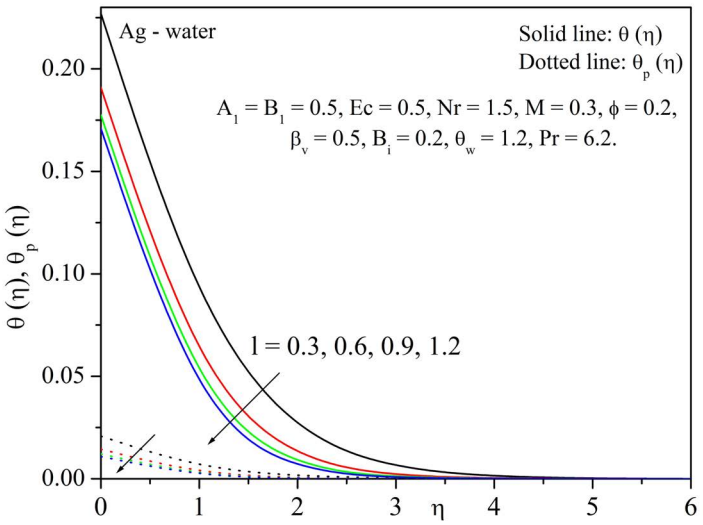

Figure 7. Temperature profile for various values of mass concentration particle parameter (l).

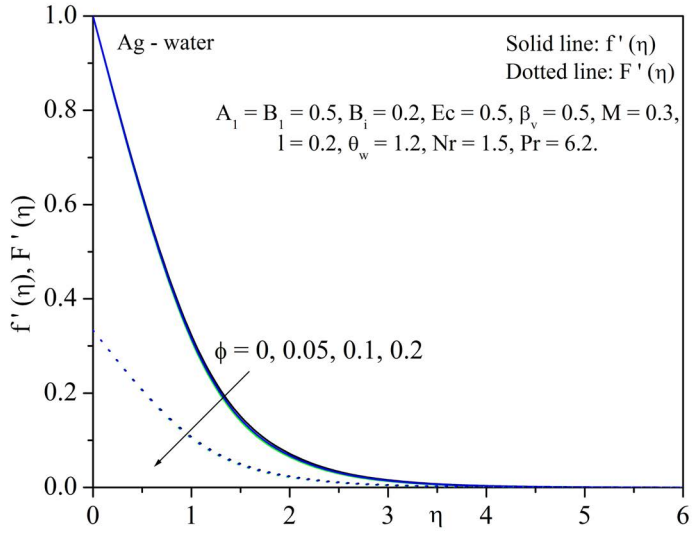

Figure 8. Velocity profile for various values of solid volume fraction parameter (ϕ).

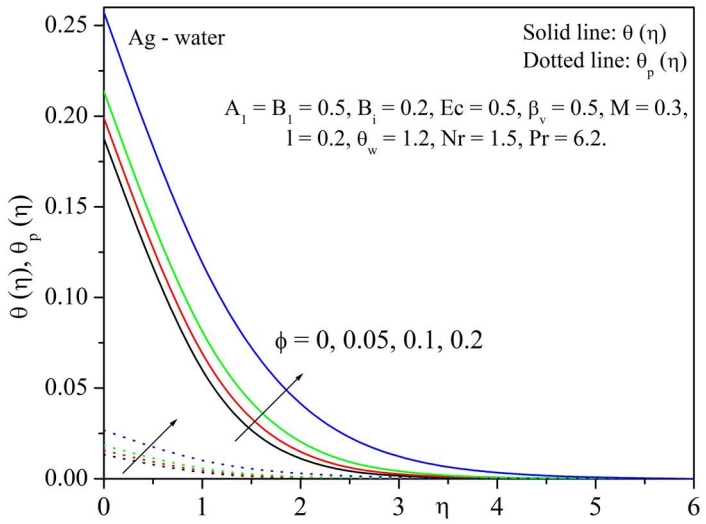

Figure 9. Temperature profile for various values of solid volume fraction parameter (ϕ).

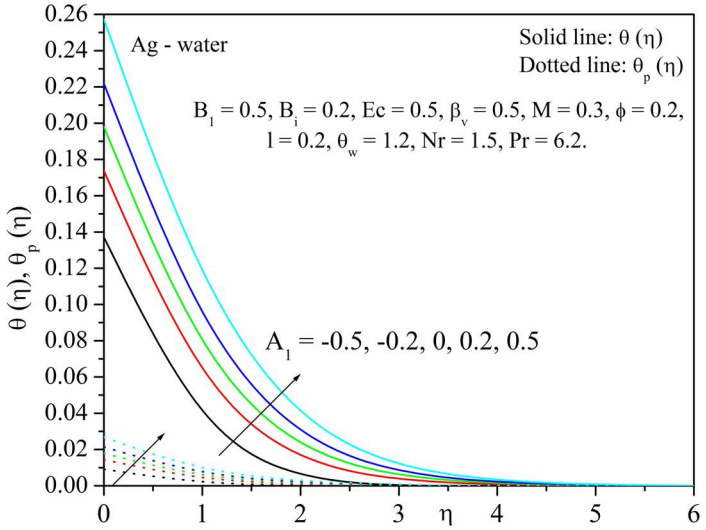

Figure 10. Temperature profile for various values of space dependent internal heat generation/absorption parameter (A_1).

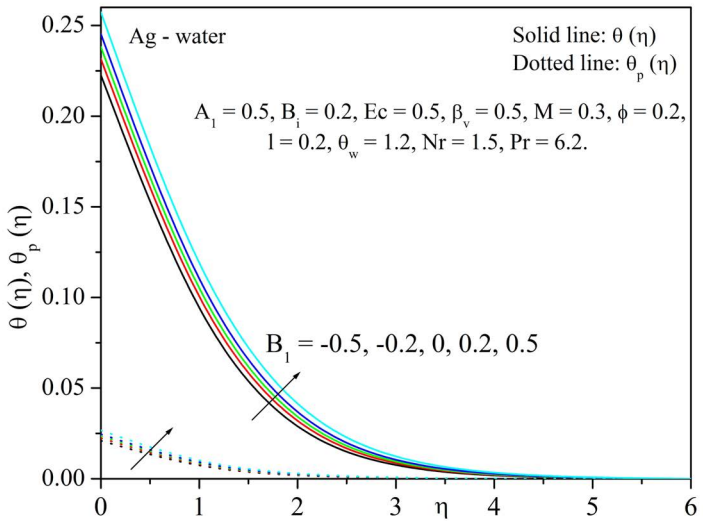

Figure 11. Temperature profile for various values of temperature dependent internal heat generation/absorption parameter (B_1).

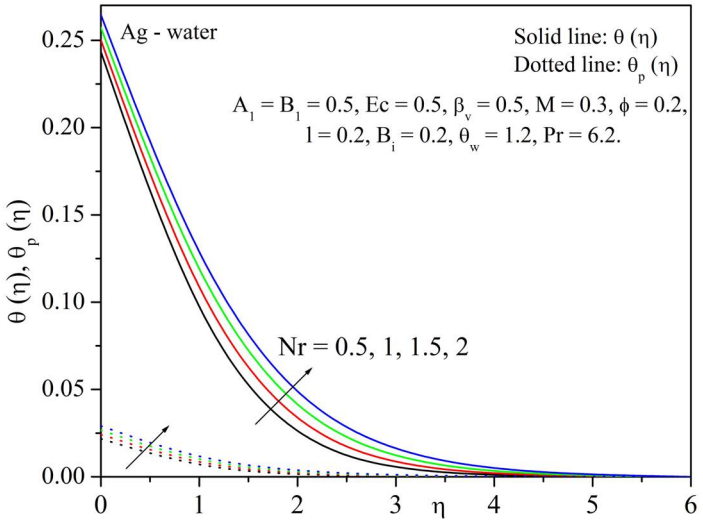

Figure 12. Temperature profile for various values of radiation parameter (Nr).

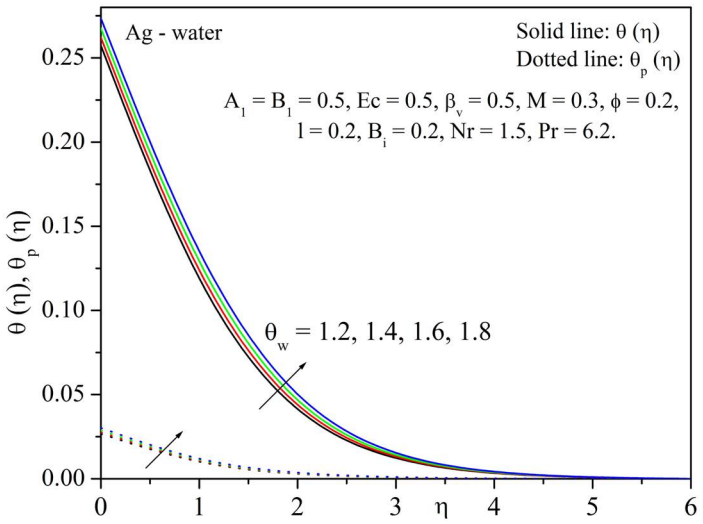

Figure 13. Temperature profile for various values of temperature ratio parameter (θ_w).

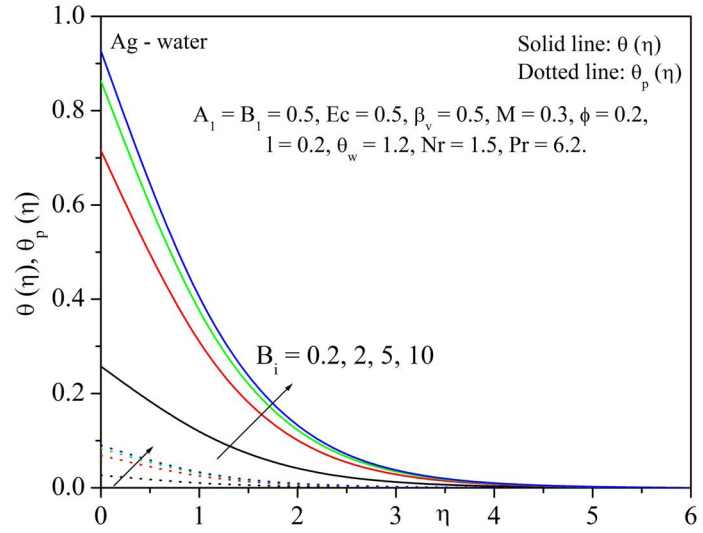

Figure 14. Temperature profile for various values of Biot number (B_i)

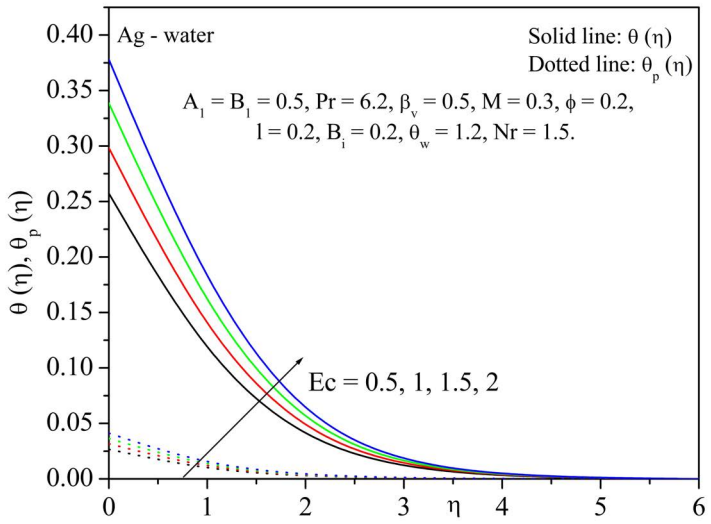

Figure 15. Temperature profile for various values of Eckert number (Ec).

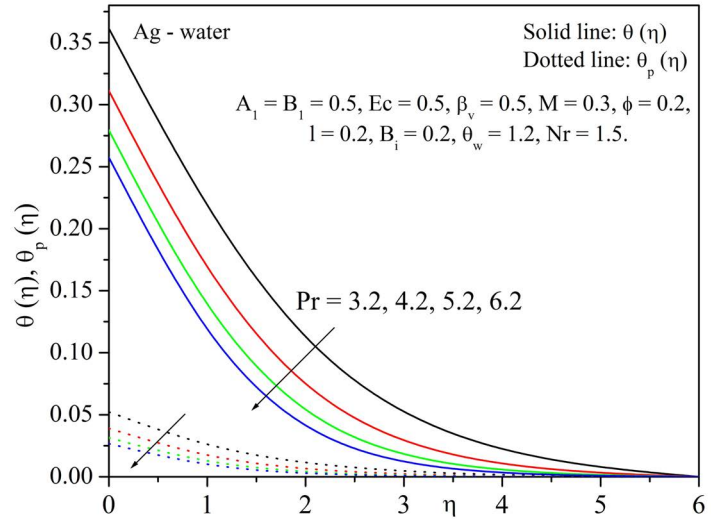

Figure 16. Temperature profile for various values of Prandtl number (Pr).

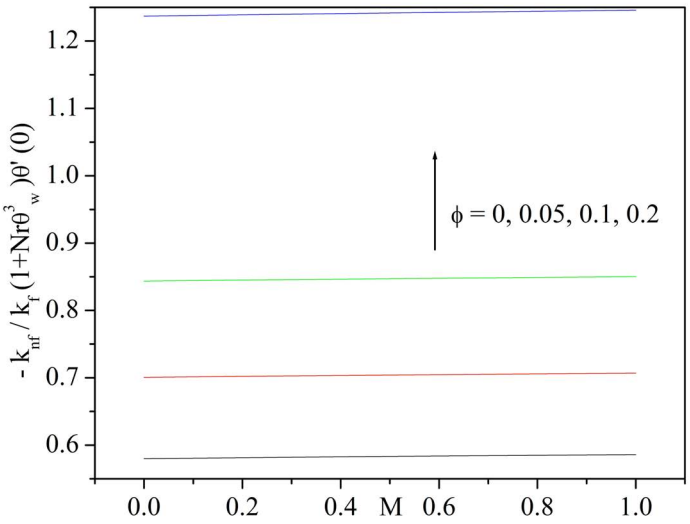

Figure 17. Effect of Nusselt number for various values of ϕ with M.

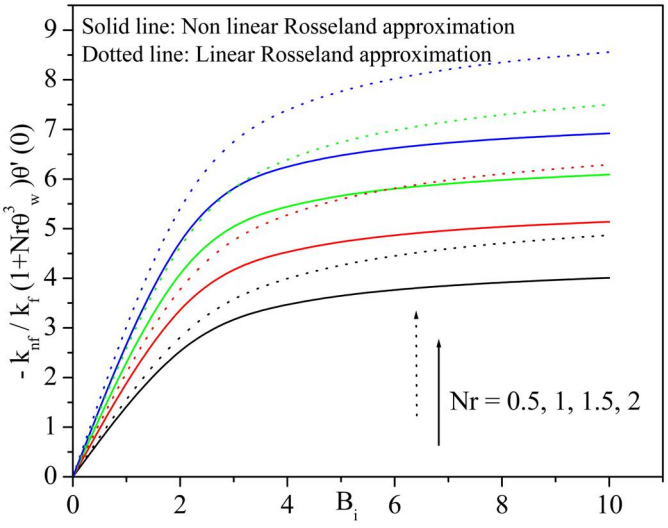

Figure 18. Effect of Nusselt number for various values of Nr with B_i.

Acknowledgements. One of the author (B. C. Prasannakumara) gratefully acknowledges the financial support of University Grants Commission (UGC), New Delhi, India [F.No-43-419/2014(SR)] for pursuing this work.

References

[1] O. A. Bég, M. J. Uddin, M. M. Rashidi, and N. Kavyani, *Double-diffusive radiative magnetic mixed convective slip flow with Biot number and Richardson number effects*, J. Eng. Thermophys. **23**(2) (2014), 79–97.

[2] C. H. Chen, *Laminar mixed convection adjacent to vertical continuously stretching sheets*, J. Heat and Mass Trans. **33** (1998), 471–476.

[3] R. Cortell, *A note on magnetohydrodynamic flow of a power-law fluid over a stretching sheet*, Appl. Math. Comput. **168** (2005), 557–566.

[4] R. Cortell, *Fluid flow and radiative nonlinear heat transfer over a stretching sheet*, J. King Saud University-Sci. **26** (2014), 161–167.

[5] L. J. Crane, *Flow past a stretching sheet*, Z. Angew. Math. Phys. (ZAMP) **21** (1970), 645–647.

[6] K. Das, *Slip flow and convective heat transfer of nanofluids over a permeable stretching surface*, Computer and Fluids **64** (2012), 34–42.

[7] N. Y. A. Elazem, A. Ebaid, and E. H. Aly, *Radiation effect of MHD on Cu water and Ag-water nanofluids flow over a stretching sheet: numerical study*, J. Appl. Computat. Math. **4**(4) (2015). 235:doi:10.4172/2168-9679.1000235.

[8] M. H. Esfe and S. Saedodin, *An experimental investigation and new correlation of viscosity of $ZnO - EG$ nanofluid at various temperatures and different solid volume fractions*. Exp. Therm. Fluid. Sci. **55** (2014), 1–5.

[9] M. H. Esfe, S. Saedodin, O. Mahian, and S. Wongwises, *Thermal conductivity of Al_2O_3-water nanofluids: measurement, correlation, sensitivity analysis and comparisons with literature reports*, J. Therm. Anal. Calorim. **117** (2014), 675–681.

[10] B. J. Gireesha, A. J. Chamkha, S. Manjunatha, and C. S. Bagewadi, *Mixed convective flow of a dusty fluid over a vertical stretching sheet with non-uniform heat source/sink and radiation*, Int. J. Num. Meth. Heat and Fluid Flow **23**(4) (2013), 598–612.

[11] R. S. R. Gorla, B. J. Gireesha, and B. Singh, *MHD flow and heat transfer of dusty nanofluid embedded in porous medium over an exponentially stretching sheet*, J. Nanofluids **4** (2015), 1–12.

[12] L. J. Grubka and K. M. Bobba, *Heat transfer characteristics of a continuous, stretching surface with variable temperature*, J. Heat Transf. **107**(1) (1985), 248–250.

[13] T. Hayat, T. Muhammada, A. Alsaedi, and M. S. Alhuthali, *Magnetohydrodynamic three-dimensional flow of viscoelastic nanofluid in the presence of nonlinear thermal radiation*, J. Magnetism and Magnetic Materials **385** (2015), 222–229.

[14] F. Hedayati, A. Malvandi, M. H. Kaffash, and D. D. Ganji, *Fully developed forced convection of alumina/water nanofluid inside microchannels with asymmetric heating*, Powder Tech. **269** (2015), 520–531.

[15] A. Ishak, *Similarity solutions for flow and heat transfer over a permeable surface with convective boundary condition*, Appl. Math. Comput. **217**(2) (2010), 837–842.

[16] P. A. K. Khare, *MHD partial slip flow of Ag-water nanofluid over a stretching sheet*, Int. J. Appl. Sci. Eng. Res. **4**(4) (2015), 557–563.

[17] F. Mabood, S. M. Ibrahim, M. M. Rashidi, M. S. Shadloo, and G. Lorenzini, *Non-uniform heat source/sink and Soret effects on MHD non-Darcian convective flow past a stretching sheet in a micropolar fluid with radiation*, Int. J. Heat and Mass Transfer **93** (2016), 674–682.

[18] A. Mahmoudi, I. Mejri, M. A. Abbassi, and A. Omri, *Analysis of MHD natural convection in a nanofluid-filled open cavity with non uniform boundary condition in the presence of uniform heat generation/absorption*, Powder Tech. **269** (2015), 275–289.

[19] O. D. Makinde and P. O. Olanrewaju, *Buoyancy effects on thermal boundary layer over a vertical plate with a convective surface boundary condition*, Trans. ASME J. Fluids Eng. **132**(4) (2010). 044502:doi:10.1115/1.4001386.

[20] A. Malvandi, F. Hedayati, and D. D. Ganji, *Boundary layer slip flow and heat transfer of nanofluid induced by a permeable stretching sheet with convective boundary condition*, J. Appl. Fluid Mech. **8**(1) (2015), 151–158.

[21] D. B. Meade, B. S. Haran, and R. E. White, *The shooting technique for the solution of two-point boundary value problems*, Maple Tech. **3** (1996), 85–93.

[22] H. A. Mintsa, G. Roy, C. T. Nguyen, and D. Doucet, *New temperature dependent thermal conductivity data for water-based nanofluids*, Int. J. Therm. Sci. **48** (2009), 363–371.

[23] R. Nandkeolyar, G. S. Seth, O. D. Makinde, P. Sibanda, and M. S. Ansari, *Unsteady hydromagnetic natural convection flow of a dusty fluid past an impulsively moving vertical plate with ramped temperature in the presence of thermal radiation*, ASME J. Appl. Mech. **680** (2013), 9 pages.

[24] A. K. Nayak, R. K. Singh, and P. P. Kulkarni, *Measurement of volumetric thermal expansion coefficient of various nanofluids*, Tech. Phys. Lett. **36** (2010), 696–698.

[25] C. T. Nguyen, F. Desgranges, N. Galanis, G. Roya, T. Maréd, S. Boucher and H. A. Mintsa, *Viscosity data for Al_2o_3-water nanofluid-hysteresis: is heat transfer enhancement using nanofluids reliable*, Int. J. Therm. Sci. **47** (2008), 103–111.

[26] B. C. Pak and Y. Cho, *Hydrodynamic and heat transfer study of dispersed fluids with submicron metallic oxide particle*, Exp. Heat. Transf. **11** (1998), 151–170.

[27] G. Palani and P. Ganesan, *Heat transfer effects on dusty gas flow past a semi-infinite inclined plate*, Forsch Ingenieurwes **71** (2007), 223–230.

[28] A. Pantokratoras and T. Fang, *Sakiadis flow with nonlinear Rosseland thermal radiation*, Physic Scrip **87**(1) (2013), 5 pages.

[29] B. C. Prasannakumara, B. J. Gireesha, R. S. R. Gorla, and M. R. Krishnamurthy, *Effects of chemical reaction and nonlinear thermal radiation on williamson nanofluid slip flow over a stretching sheet embedded in a porous medium*, J. Aerosp. Eng. **29**(5) (2016). 04016019:doi:10.1061/(ASCE)AS.1943-5525.0000578.

[30] G. K. Ramesh and B. J. Gireesha, *Influence of heat source/sink on a Maxwell fluid over a stretching surface with convective boundary condition in the presence of nanoparticles*, Ain Shams Eng. J. **5**(3) (2014), 991–998.

[31] S. Rosseland, in: *Astrophysik und atom-theoretische Grundlagen*, Springer-Verlag, Berlin, 1931, pp. 41–44.

[32] P. G. Saffman, *On the stability of laminar flow of a dusty gas*, J. Fluid Mech. **13** (1962), 120–128.

[33] B. C. Sakiadis, *Boundary layer behaviour on continuous solid surface*, AICh. E. J. **7** (1961), 26–28.

[34] H. Schlichting and H. Gersten, *Boundary-layer Theory*, Springer, New York, 2000.

[35] S. Seigel and J. R. Howell, *Thermal Radiation Heat Transfer*, 2nd ed., McGraw-Hill Inc., New York, 1981.

[36] S. A Shehzad, F. E. Alsaadi, S. J. Monaquel, and T. Hayat, *Soret and Dufour effects on the stagnation point flow of Jeffery fluid with convective boundary conditions*, Eur. Phys. J. Plus **128** (2013). 56:https:doi.org/10.1140/epjp/i2013-13056-6

[37] M. Sheikholeslami, M. M. Rashidi and D. D. Ganji, *Effect of non-uniform magnetic field on forced convection heat transfer of Fe_3o_4 -water nanofluid*, Computer Methods Appl. Mech. Eng. **294** (2015), 299–312.
[38] D. Wen and Y. Ding, *Experimental investigation into convective heat transfer of nanofluids at the entrance region under laminar flow conditions*, Int. J. Heat Mass Transf. **47** (2004), 5181–5188.
[39] Y. Xuan and Q. Li, *Investigation on convective heat transfer and flow features of nanofluids*, J. Heat Transf. **125** (2003), 151–155.

Department of Studies and Research in Mathematics, Kuvempu University, Shankaraghatta-577 451, Shimoga, Karnataka, India
E-mail address: bjgireesu@gmail.com

Department of Mechanical Engineering, Cleveland State University, Cleveland, Ohio-44115, USA
E-mail address: rgorla@pnw.edu

Department of Mathematics, Jawaharlal Nehru National College of Engineering, Shimoga-577201, Karnataka, India
E-mail address: kittysa.mr@gmail.com

Government First Grade College, Koppa, Chikkamagaluru-577126, Karnataka, India
E-mail address: dr.bcprasanna@gmail.com